Air quality and radiative forcing impacts of anthropogenic volatile organic compound emissions from ten world regions

M. M. Fry[1,*]**, M. D. Schwarzkopf**[2]**, Z. Adelman**[1]**, and J. J. West**[1]

[1]Department of Environmental Sciences and Engineering, University of North Carolina at Chapel Hill, Chapel Hill, North Carolina, USA
[2]NOAA Geophysical Fluid Dynamics Laboratory, Princeton, New Jersey, USA
[*]now at: US Environmental Protection Agency, Washington, DC, USA

Correspondence to: J. J. West (jjwest@email.unc.edu)

Abstract. Non-methane volatile organic compounds (NMVOCs) influence air quality and global climate change through their effects on secondary air pollutants and climate forcers. Here we simulate the air quality and radiative forcing (RF) impacts of changes in ozone, methane, and sulfate from halving anthropogenic NMVOC emissions globally and from 10 regions individually, using a global chemical transport model and a standalone radiative transfer model. Halving global NMVOC emissions decreases global annual average tropospheric methane and ozone by 36.6 ppbv and 3.3 Tg, respectively, and surface ozone by 0.67 ppbv. All regional reductions slow the production of peroxyacetyl nitrate (PAN), resulting in regional to intercontinental PAN decreases and regional NO_x increases. These NO_x increases drive tropospheric ozone increases nearby or downwind of source regions in the Southern Hemisphere (South America, Southeast Asia, Africa, and Australia). Some regions' NMVOC emissions contribute importantly to air pollution in other regions, such as East Asia, the Middle East, and Europe, whose impact on US surface ozone is 43 %, 34 %, and 34 % of North America's impact. Global and regional NMVOC reductions produce widespread negative net RFs (cooling) across both hemispheres from tropospheric ozone and methane decreases, and regional warming and cooling from changes in tropospheric ozone and sulfate (via several oxidation pathways). The 100 yr and 20 yr global warming potentials (GWP_{100}, GWP_{20}) are 2.36 and 5.83 for the global reduction, and 0.079 to 6.05 and −1.13 to 18.9 among the 10 regions. The NMVOC RF and GWP estimates are generally lower than previously modeled estimates, due to the greater $NMVOC/NO_x$ emissions ratios simulated, which result in less sensitivity to NMVOC emissions changes and smaller global O_3 burden responses, in addition to differences in the representation of NMVOCs and oxidation chemistry among models. Accounting for a fuller set of RF contributions may change the relative magnitude of each region's impacts. The large variability in the RF and GWP of NMVOCs among regions suggest that regionally specific metrics may be necessary to include NMVOCs in multi-gas climate trading schemes.

1 Introduction

Non-methane volatile organic compounds (NMVOCs) are chemically reactive gases emitted worldwide from natural and anthropogenic sources. NMVOCs impact air quality and climate by contributing to tropospheric photochemistry (e.g., ozone (O_3) production) and aerosol formation. Because of their influence on short-lived climate forcers (e.g., O_3, methane (CH_4), aerosols), NMVOC reductions could help slow the near-term rate of climate change (Shindell et al., 2012). Here we evaluate the net climate and air quality effects of anthropogenic NMVOC emission reductions, to inform future policies that may address air quality and climate change.

Tropospheric CH_4 and O_3 are the largest greenhouse gas contributors to global anthropogenic radiative climate forcing (RF) behind carbon dioxide (CO_2) with abundance-based RFs of 0.48 ± 0.05 W m^{-2} and 0.35 (-0.1, $+0.3$) W m^{-2},

respectively (Forster et al., 2007). Tropospheric sulfate (SO_4^{2-}) has produced a global net RF of $-0.40 \pm 0.2\,\mathrm{W\,m^{-2}}$ (direct effect only) (Forster et al., 2007). NMVOCs and carbon monoxide (CO) emissions together have contributed an estimated global mean RF of $0.21 \pm 0.10\,\mathrm{W\,m^{-2}}$ due to O_3 and CH_4 (1750 to 1998) (Shindell et al., 2005; Forster et al., 2007) and $0.25 \pm 0.04\,\mathrm{W\,m^{-2}}$ (1750 to 2000) when SO_4^{2-}, nitrate (NO_3^-), and CO_2 impacts are included (Shindell et al., 2009). More recently, the anthropogenic RF of NMVOC emissions (for 1850–2000) was estimated as $0.090\,\mathrm{W\,m^{-2}}$ (due to changes in O_3, CH_4, and CO_2) as part of the Atmospheric Chemistry and Climate Model Intercomparison Project (ACCMIP) (Stevenson et al., 2013).

NMVOCs are oxidized by the hydroxyl radical (OH) in the troposphere, producing peroxyl radicals (RO_2) and hydroperoxy radicals (HO_2) that then oxidize nitric oxide (NO) to yield O_3. Other reactants (e.g., O_3 and NO_3 radicals) also contribute to oxidation reactions. Because thousands of NMVOC species with varying lifetimes (from fractions of a day to months) and chemical reactivities have been documented, global chemical transport models (CTMs) use simplified representations of NMVOCs and reaction pathways (Ehhalt et al., 2001; Prather et al., 2001; Ito et al., 2007). Under high nitrogen oxide ($NO_x = NO + NO_2$) concentrations, NMVOCs contribute to the efficient cycling between OH and HO_2 and hence, O_3 production, while under low-NO_x conditions OH depletes, resulting in NMVOC and methane (CH_4) accumulation (Collins et al., 2002). CH_4 is a longer-lived O_3 precursor (perturbation lifetime of $\sim$12 yr) (Forster et al., 2007) that decreases as tropospheric OH increases (from NMVOC reductions), resulting in long-term O_3 decreases, in addition to direct, short-term O_3 decreases (Prather et al., 1996; Wild et al., 2001; Fiore et al., 2002; Naik et al., 2005). NMVOC emissions also affect O_3 at local to intercontinental scales, given that the lifetimes of tropospheric O_3 ($\sim$22 days) (Stevenson et al., 2006) and some NMVOCs (e.g., ethane, benzene) can exceed typical intercontinental transport times (5 to 10 days) (Fiore et al., 2009; West et al., 2009a). NMVOC reductions indirectly influence sulfate aerosol (SO_4^{2-}) formation via gas-phase oxidation of sulfur dioxide (SO_2) by OH, and aqueous-phase oxidation of SO_2 by H_2O_2 or O_3 (Unger et al., 2006; Leibensperger et al., 2011). NMVOCs are also precursors to secondary organic aerosols (SOA), and influence NO_3^- aerosol abundance via oxidant changes (Ehhalt et al., 2001; Bauer et al., 2007; Hoyle et al., 2009).

Previous studies have shown that the RF and global warming potential (GWP) of NMVOCs, like other short-lived O_3 precursors, depend on emissions location given their short lifetime in the troposphere (Naik et al., 2005; Berntsen et al., 2006; Forster et al., 2007; Fry et al., 2012), but few studies quantify the range among different source regions. Fry et al. (2012) calculated 100 yr and 20 yr GWPs (GWP$_{100}$, GWP$_{20}$) of 4.8 ± 2.4 to 8.3 ± 1.9 and 15.5 ± 6.8

to 26.5 ± 5.3, respectively, for anthropogenic NMVOCs from four regions (due to O_3, CH_4, and SO_4^{2-}) using an ensemble of models. Collins et al. (2002) also presented GWP$_{100}$ estimates of 1.8 to 5.5 (-50 to $+100\,\%$ uncertainty) due to CH_4 and O_3, but for individual anthropogenic NMVOCs globally.

Using global models of chemical transport and radiative transfer, we simulate the air quality and net RF impacts, via changes in O_3, CH_4, and SO_4^{2-}, of halving all anthropogenic NMVOC emissions together, globally and from 10 regions, as was done for CO emissions by Fry et al. (2013). We evaluate the sensitivity of air quality and RF to NMVOC emission location, and the corresponding NMVOC GWPs, which may support the inclusion of NMVOCs in multi-gas emission trading schemes for climate. We do not consider reductions in co-emitted species that would be affected by measures to reduce NMVOCs. Future studies could evaluate the impacts of measures on multiple species, or combine the results presented here with those for co-emitted species to determine the net effect of emission control measures (Shindell et al., 2012).

2   Methods

2.1   Global chemical transport model

We evaluate the impacts on surface air quality and tropospheric composition of halving anthropogenic NMVOC emissions globally and from 10 regions (North America (NA), South America (SA), Europe (EU), the former Soviet Union (FSU), Southern Africa (AF), India (IN), East Asia (EA), Southeast Asia (SE), Australia and New Zealand (AU), and the Middle East and Northern Africa (ME)) (Fig. S1) (Fry et al., 2013). We use the global chemical transport model (CTM), Model for OZone And Related chemical Tracers version 4 (MOZART-4) (Emmons et al., 2010).

The base and CH_4 control (where global CH_4 was reduced by 20 %) simulations are documented in a previous study in which the base simulation was shown to generally agree with surface and tropospheric observations (Fry et al., 2013). Here we simulate new perturbation experiments that reduce regional and global anthropogenic NMVOC emissions by 50 % for 1 July 2004 through 31 December 2005 using MOZART-4 at a horizontal resolution of 1.9° latitude × 2.5° longitude with 56 vertical levels. We use the Coupled Model Intercomparison Project phase 5 (CMIP5) Representative Concentration Pathway 8.5 (RCP8.5) emissions inventory for the year 2005 (Riahi et al., 2007, 2011) and global meteorology from the Goddard Earth Observing System Model, version 5 (GEOS-5) (2004 to 2006) (Rienecker et al., 2008). Anthropogenic emissions include all anthropogenic sectors except biomass burning emissions (Fig. S2), which are excluded since actions to address biomass burning (i.e., reductions in burning) differ from the other anthropogenic sectors (Naik et al., 2007), and would likely reduce the emissions of

all co-emitted species by similar percentages. Actions to reduce anthropogenic emissions from industrial sources, on the other hand, likely have differing effects on NMVOCs relative to other co-emitted species.

RCP8.5 NMVOC species are re-speciated to MOZART-4 NMVOC categories, and monthly temporal variation is added to all anthropogenic species and source categories, except for shipping, aircraft, and biomass burning, which already have monthly temporal variation (Fig. S2, Table S1). The Model of Emissions of Gases and Aerosols from Nature (MEGAN) (Guenther et al., 2006) within MOZART-4 calculates the biogenic emissions of isoprene and monoterpenes ($C_{10}H_{16}$) (global annual totals of $738 \, \mathrm{Tg \, C \, yr^{-1}}$ and $107 \, \mathrm{Tg \, C \, yr^{-1}}$, respectively), while all other natural emissions are from Emmons et al. (2010) (Table S2). The global annual lightning NO_x and soil NO_x emissions are also calculated by MOZART-4 as $2.4 \, \mathrm{Tg \, N \, yr^{-1}}$ and $8.0 \, \mathrm{Tg \, N \, yr^{-1}}$ (Fry et al., 2013).

Because the perturbation simulations are only 1.5 yr in length, we account for the influence of NMVOC emissions on CH_4 (via OH), and thus long-term changes in O_3 on the decadal timescale of the CH_4 perturbation lifetime, using methods from previous studies (Prather et al., 2001; West et al., 2007; Fiore et al., 2009; Fry et al., 2012). Global CH_4 is set to a uniform mixing ratio of 1783 parts per billion by volume (ppbv) (WMO, 2006) in the base and perturbation simulations. The CH_4 control simulation reduced global CH_4 to 1426.4 ppbv. The results from the base and CH_4 control simulations were used by Fry et al. (2013) to estimate CH_4 lifetime against loss by tropospheric OH (τ_{OH}, 11.24 yr), total CH_4 lifetime based on τ_{OH} and CH_4 loss to soils and the stratosphere (τ_{total}, 9.66 yr), and methane's feedback factor (F, 1.29) by the methods of Prather et al. (2001) and Stevenson et al. (2013). We use these parameters to estimate the steady-state tropospheric CH_4 change for each of the NMVOC perturbations. Long-term O_3 responses are then calculated offline by scaling O_3 changes from the CH_4 control simulation by the ratio of the global CH_4 change from each perturbation to that of the CH_4 control. We add long-term O_3 changes to direct short-term O_3 changes to estimate the net change at steady state (West et al., 2007, 2009b; Fiore et al., 2009; Fry et al., 2012).

Since MOZART-4 does not have complete stratospheric chemistry (Emmons et al., 2010), we merge each simulation's steady-state (short-term + long-term) tropospheric O_3 distributions (in three dimensions) with the monthly mean stratospheric O_3 concentrations from the AC&C/SPARC (Stratospheric Processes And their Role in Climate) O_3 database prepared for CMIP5 (Available: http://pcmdi-cmip.llnl.gov/cmip5/forcing.html) (Cionni et al., 2011). By omitting lower stratospheric O_3 changes between each perturbation and the base simulation, our RF estimates likely underestimate the full effect of NMVOC emissions (Søvde et al., 2011).

MOZART-4 accounts for the tropospheric aerosols SO_4^{2-}, black carbon (BC), primary and secondary organics, NO_3^-, dust, and sea salt aerosols (Lamarque et al., 2005). Here we focus on changes in SO_4^{2-}, NO_3^-, and SOA, as these species are most directly influenced by anthropogenic NMVOCs, where NMVOCs are precursors to SOA, and changes in oxidants affect all three aerosol species (Barth et al., 2000; Metzger et al., 2002; Chung and Seinfeld, 2002).

2.2 Radiative transfer model

We use the NOAA Geophysical Fluid Dynamics Laboratory (GFDL) standalone radiative transfer model (RTM) to perform stratospheric-adjusted net RF calculations (Schwarzkopf and Ramaswamy, 1999; GFDL GAMDT, 2004; Naik et al., 2005, 2007) as in Fry et al. (2012), with the same updates to long-lived greenhouse gases (Meinshausen et al., 2011) and solar forcing (http://www.geo.fu-berlin.de/en/met/ag/strat/forschung/SOLARIS/Input_data/CMIP5_solar_irradiance.html) from Fry et al. (2013). Net RF is calculated as the difference between the perturbed and base cases' simulated monthly mean net radiation fluxes (net shortwave minus net longwave), in each grid cell and month, at the tropopause after stratospheric temperatures have readjusted to radiative equilibrium (Naik et al., 2007; Saikawa et al., 2009; Fry et al., 2012). We quantify the net RF from changes in tropospheric steady-state O_3, CH_4, and SO_4^{2-} (direct effect only), as modeled by the MOZART-4 simulations. Meteorological fields from GFDL's atmosphere model (AM2) and land model (LM2), sampled one day per month at midmonth for the year 2005, are also used as input to the RTM simulations, representing monthly mean conditions (Naik et al., 2005).

The RTM currently does not calculate the RF of SOA and NO_3^- aerosols. We also do not account for the RF of changes in stratospheric O_3, water vapor, the carbon cycle (via O_3 and nitrogen deposition, affecting plants), and CO_2 (via NMVOC oxidation, which has a minor influence on the net RF of NMVOCs) (Shindell et al., 2009). We do not estimate CO_2 forcing here, because this carbon is likely accounted for in CO_2 inventories (Daniel and Solomon, 1998). Our RTM simulations also exclude the indirect effects of aerosols on clouds and the internal mixing of aerosols, where aerosol indirect effects are highly uncertain and may account for considerable RF beyond aerosol direct effects (Forster et al., 2007; Shindell et al., 2013).

3 Tropospheric composition and surface air quality

3.1 Methane and ozone

Global annual average changes in steady-state tropospheric CH_4 abundance, calculated from the tropospheric CH_4 loss flux diagnosed from the model (West et al., 2007; Fiore et al., 2009; Fry et al., 2013), are largest for ME (-7.37 ppbv)

Table 1. Changes in global annual average short-term and steady-state tropospheric O_3 burden (B_{O_3}) and tropospheric CH_4 for the global and regional reductions. Changes in O_3 production (P_{O_3}), P_{O_3} normalized per unit change in NMVOC emissions (E), and P_{O_3} outside each reduction region are shown for each regional reduction. Changes in net O_3 export (X_{O_3}) from each reduction region, and the fractions of B_{O_3} and P_{O_3} changes above each reduction region are also estimated.

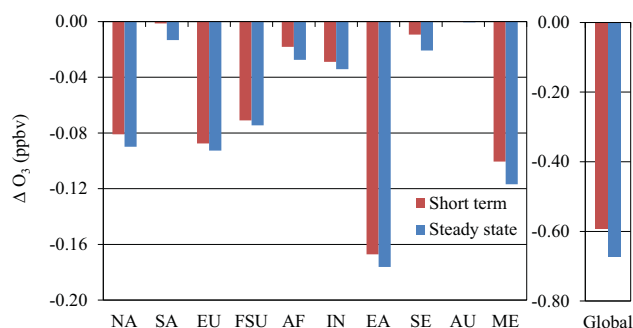| Reduction region	ΔB_{O_3} (Tg O_3) short-term	ΔB_{O_3} (Tg O_3) steady-state	$\Delta B_{O_3}/\Delta E$ (Tg O_3 (Tg C yr^{-1})$^{-1}$) steady-state	ΔCH_4 (ppbv)	$\Delta CH_4/\Delta E$ (ppbv (Tg C yr^{-1})$^{-1}$)	ΔP_{O_3} (Tg yr^{-1})	$\Delta P_{O_3}/\Delta E$ (Tg O_3 (Tg C yr^{-1})$^{-1}$)	ΔP_{O_3} outside region (Tg yr^{-1})	ΔX_{O_3} from region (Tg yr^{-1})	Fraction of global ΔB_{O_3} above region	Fraction of global ΔP_{O_3} above region
NA	−0.30	−0.41	0.082	−4.05	0.80	−6.13	1.21	−3.92	−0.84	0.19	0.36
SA	0.16	0.028	−0.008	−5.41	1.60	1.95	−0.58	0.67	0.72	0.13	0.66
EU	−0.31	−0.38	0.101	−2.30	0.61	−6.15	1.64	−4.17	−1.19	0.087	0.32
FSU	−0.21	−0.25	0.101	−1.61	0.64	−3.80	1.52	−2.83	−0.48	0.21	0.25
AF	−0.081	−0.20	0.049	−4.20	1.03	−2.22	0.54	−2.34	0.41	−0.041	−0.052
IN	−0.23	−0.30	0.081	−2.40	0.65	−5.09	1.38	−3.14	−0.67	0.071	0.38
EA	−0.90	−1.02	0.099	−4.10	0.40	−18.6	1.82	−11.2	−3.79	0.10	0.40
SE	0.075	−0.066	0.016	−5.16	1.22	−0.18	0.04	−1.40	0.80	0.21	−6.75
AU	0.013	0.00	0.000	−0.54	1.61	0.19	−0.58	0.20	−0.014	0.040	−0.032
ME	−0.50	−0.69	0.091	−7.37	0.97	−9.48	1.24	−6.31	−1.79	0.10	0.33
Global	−2.44	−3.33	0.073	−36.6	0.81	−52.1	1.15	–	–	–	–

Table 2. For the global and regional reduction simulations relative to the base, global annual average changes in short-term and steady-state surface O_3.

| Reduction region	ΔSurface O_3 short term (pptv)	ΔSurface O_3 steady state (pptv)
NA	-81.0	-89.9
SA	-1.40	-13.3
EU	-87.5	-92.6
FSU	-71.0	-74.5
AF	-18.2	-27.5
IN	-28.9	-34.2
EA	-167.1	-176.2
SE	-9.40	-20.8
AU	0.60	-0.60
ME	-100.6	-116.8
Global	-592.9	-673.5

Fig. 1. Global annual average surface O_3 concentration changes (ppbv) for the regional and global reduction simulations, in the short term and at steady state.

and SA (-5.41 ppbv) reductions among the 10 regions (Table 1). Normalized global CH_4 changes range from 0.40 to 1.61 ppbv CH_4 $(Tg\,C\,yr^{-1})^{-1}$ among the 10 regions, and are most sensitive to reductions from AU, SA, SE, and AF. These are regions of low NO_x, as discussed below, where reducing NMVOCs lessens OH depletion, creating greater global CH_4 changes per unit emission. CH_4 decreases are least sensitive to NMVOC reductions from high-NO_x regions (EA, EU, FSU). Naik et al. (2005) also found greater global CH_4 sensitivities for NO_x emissions from low-NO_x regions (SE, SA, and AU), and lower sensitivities for high-NO_x regions (EU, FSU).

Global short-term and steady-state surface O_3 changes for the 10 regional reductions are nearly proportional to NMVOC emissions changes ($R^2 = 0.69$ and 0.81) (Fig. S3), but not as strongly correlated as for regional CO reductions (Fry et al., 2013). NMVOC emissions produce long-term O_3 decreases that augment short-term decreases by 13 % for the global reduction, and by 5–18 % for the regional reductions (Fig. 1, Table 2), similar to Fiore et al. (2009) and West et al. (2007). SA, AF, and SE reductions provide more substantial long-term global surface O_3 changes, which account for ~34 to 89 % of steady-state O_3 decreases.

Several of the regional reductions (SA, AF, SE, and AU) in the tropics and Southern Hemisphere (SH) produce regional to intercontinental tropospheric O_3 column increases (Fig. 2), as the sensitivity of O_3 to NMVOC emissions varies by world region. All of the regional reductions slow the formation of peroxyacetyl nitrate (PAN), causing PAN to decrease regionally to hemispherically and NO_x to increase regionally (Figs. S5, S6, and S7). For SA, AF, SE, and AU, these NO_x increases cause O_3 column increases near or downwind of the region. For the other regions, decreases in NMVOCs decrease O_3, outweighing the influence of NO_x increases via slowing PAN production. Whether NMVOC reductions cause O_3 to increase or decrease de-

pends on the regional chemical state. Here O_3-NO_x-VOC sensitivity is analyzed using the photochemical indicator ratios: $P(H_2O_2)/P(HNO_3)$, where $P()$ refers to production rate, $(H_2O_2)/(HNO_3)$, and $(H_2O_2)/(NO_2)$ (Sillman et al., 1997; Liu et al., 2010). The modeled indicator ratios show that NO_x-sensitive conditions prevail in the tropics and southern midlatitudes, supporting the finding of tropospheric O_3 increases from SA, AF, SE, and AU reductions (Figs. S8, S9, and S10). The northern mid- to high latitudes more frequently exhibit VOC sensitivity (weaker NO_x sensitivity), particularly from November to March, resulting in O_3 decreases.

The global distributions of steady-state surface and tropospheric O_3 show the greatest decreases within each reduction region, and smaller decreases intercontinentally (Figs. 2, S4, and Table S3). Although the largest changes in surface O_3 occur within the hemisphere of reduction, given that interhemispheric transport takes ~1 year (Jacob, 1999), more widespread decreases reflect global long-term O_3 decreases (via CH_4 decreases). NMVOC reductions in one region can also influence surface O_3 concentrations in other regions importantly (Tables S3 and S4). In fact, the EA, ME, and EU NMVOC reductions have an impact on US surface O_3 that is 43 %, 34 %, and 34 %, respectively, of that from the NA reduction. Two of the low-NO_x regions (SA and SE) experience greater decreases in surface O_3 from foreign regions' NMVOCs than domestic NMVOCs.

The global annual average steady-state tropospheric O_3 burden decreases by 0.073 Tg O_3 $(Tg\,C\,yr^{-1})^{-1}$ for the global reduction and by -0.008 to 0.101 Tg O_3 $(Tg\,C\,yr^{-1})^{-1}$ for the 10 regions (Table 1). Changes in O_3 production (ΔP) and export (ΔX) are also calculated to determine the importance of long-range transport of O_3 and its precursors. For most regions, changes in O_3 production outside of each reduction region exceed changes in O_3 export from each region, suggesting that the influence of NMVOC emissions on the downwind production of O_3 has a greater impact on long-range O_3 than the formation and export of O_3 from each region (Table 1). In contrast, for the SA, AF, and
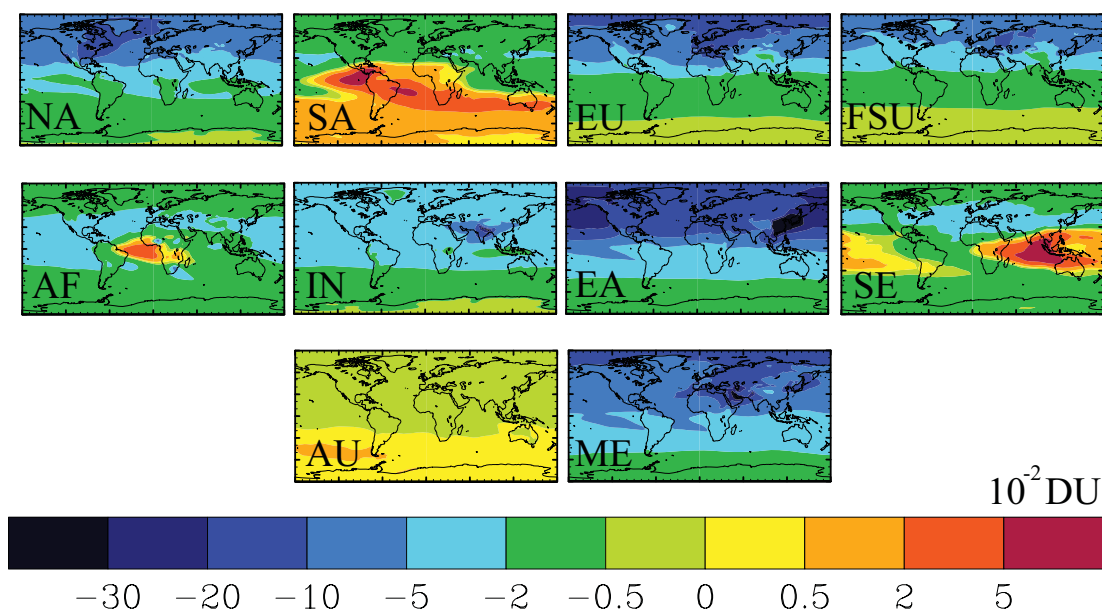
Fig. 2. Global distribution of annual average changes in tropospheric total column O_3 at steady state (1×10^{-2} DU) for each of the regional reduction simulations relative to the base.
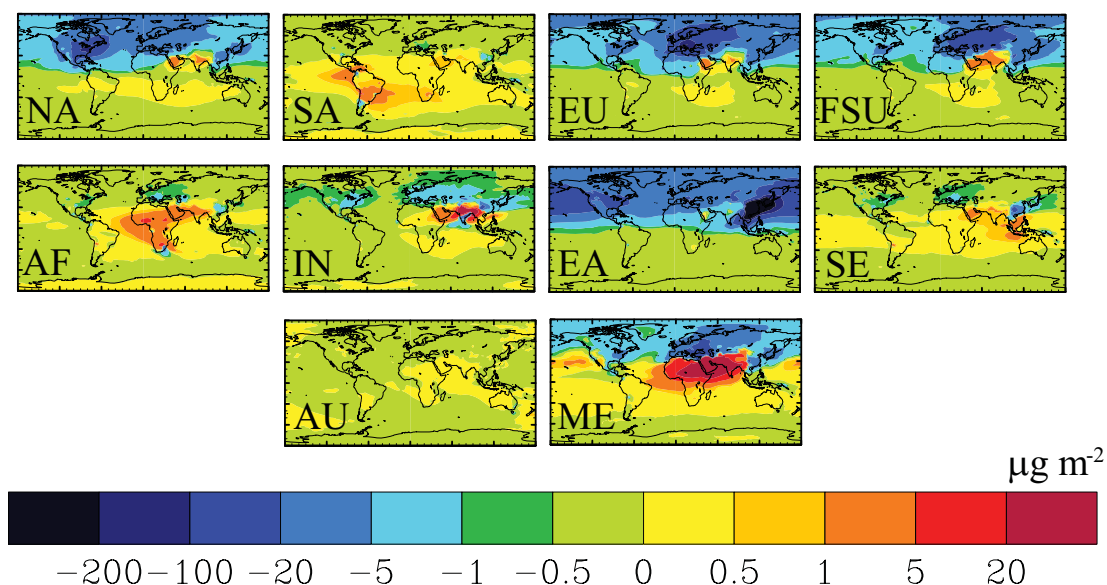
Fig. 3. Global distribution of annual average changes in tropospheric total column SO_4^{2-} ($\mu g\, m^{-2}$) for each of the regional reduction simulations relative to the base.

SE reductions, ΔX is positive due to regional O_3 increases. O_3 production outside the reduction region decreases for AF and SE, yet increases for SA, as SA causes widespread increases in tropospheric O_3 (Fig. 2). For AU, regional tropospheric O_3 export decreases, while tropospheric O_3 production increases outside AU (Table 1, Fig. 2).

3.2   Aerosols

NMVOC reductions affect the oxidation of SO_2, NO_x, monoterpenes, and toluene, influencing tropospheric SO_4^{2-}, NO_3^-, and SOA concentrations. Reductions from regions near the Equator and in drier areas (SA, AF, IN, SE, and ME) produce widespread SO_4^{2-} increases (Fig. 3), related to increased gas-phase SO_2 oxidation by OH. In fact, most of the regional reductions, except EA and AU, produce localized increases in SO_4^{2-} over drier areas (e.g., the Middle East and

Table 3. For the global and regional reduction simulations relative to the base, global annual average tropospheric burden changes in SO_4^{2-}, NO_3^- (expressed as NH_4NO_3), and SOA. The global annual average tropospheric SO_4^{2-}, NH_4NO_3, and SOA burdens in the base simulation are $1785\,Gg\,SO_4^{2-}$, $416\,Gg\,NH_4NO_3$, and $227\,Gg\,SOA$.

Reduction region	ΔSO_4^{2-} (Gg)	ΔNH_4NO_3 (Gg)	ΔSOA (Gg)
NA	−1.63	0.61	−2.91
SA	0.05	0.17	−4.57
EU	−2.26	1.47	−1.30
FSU	−1.45	0.88	−0.74
AF	0.06	0.21	−2.84
IN	−0.03	0.05	−1.66
EA	−10.3	3.21	−3.69
SE	−0.06	0.38	−5.00
AU	−0.01	0.01	−0.25
ME	1.63	0.09	−1.89
Global	−14.8	7.27	−24.9

India). Tropospheric O_3 increases from the SA, AF, and SE reductions also contribute to SO_4^{2-} increases via enhanced aqueous-phase SO_2 oxidation by O_3, where aqueous-phase SO_2 oxidation is more efficient than gas-phase oxidation (Unger et al., 2006). Regional reductions in the northern mid-latitudes (NA, EU, FSU, and EA) result in widespread decreases in SO_4^{2-}, due to the prevalence of clouds and decreased aqueous-phase oxidation (in clouds) of SO_2 by O_3 and H_2O_2 (Figures 3, S11, and S12). NO_3^- changes include both regional increases and decreases. As with SO_4^{2-}, NO_3^- increases are expected due to OH increases that are global in scale, yet largest over the source region (Figures S13 and S14). SOA decreases globally, influenced not only by oxidant changes, but also by NMVOCs directly, as NMVOCs are precursors to SOA. The largest SOA decreases occur over the reduction region (Fig. S15). While MOZART-4 accounts for SOA formation through the oxidation of monoterpenes and toluene, more research is needed to more fully model SOA. Current models greatly simplify the physical and chemical processes contributing to SOA burden, and underpredict SOA formation compared to observations (Carlton et al., 2009).

Global annual average SO_4^{2-} burden decreases for most regional reductions, yet increases for SA, AF, and ME (Table 3). For all 10 regional reductions, global NO_3^- burden increases and global SOA burden decreases. The sums of global burden changes for all 10 regional reductions, for SO_4^{2-}, NO_3^-, and SOA, are 95 to 99 % of the burden changes for the global NMVOC reduction, suggesting some dependence on regional conditions and chemistry.

Summing the effects of individual aerosol species shows that the greatest changes in fine particulate matter ($PM_{2.5}$, estimated as a sum not including dust and sea salt) occur within the reduction region, and extend intercontinentally in some cases (Fig. S16). Halving global NMVOC emissions slightly decreases global and regional annual average surface $PM_{2.5}$ concentrations (Table S7). Regional NMVOC reductions also have a small influence on surface $PM_{2.5}$ concentrations in other regions (Table S8, S9), but halving NMVOCs generally does not have a strong influence on $PM_{2.5}$ air quality, with changes smaller than the accuracy of the model and measurements.

4 Radiative forcing and global warming potential

The global annual average net RF is estimated as $-9.73\,mW\,m^{-2}$ for the global 50 % NMVOC reduction or $0.21\,mW\,m^{-2}\,(Tg\,C\,yr^{-1})^{-1}$ (Table 4). This estimate for the global NMVOC reduction differs somewhat from the sum of the 10 regions' global net RF estimates ($12.5\,mW\,m^{-2}$) (Table 4), suggesting some level of error in adding the ten regions' net RF impacts to get a global total net RF. However, in order to compare with other estimates of anthropogenic forcing, we estimate the global net RF by multiplying each region's global net RF per unit emissions (Table 4) by total anthropogenic emissions including biomass burning, which were excluded in the 50 % reductions (Table S2). We then sum the ten regions' global net RF estimates to yield $0.0374\,W\,m^{-2}$ as the net RF of anthropogenic NMVOCs.

This approach accounts for the geographic variability of biomass burning emissions, yet assumes the same mixture of NMVOC species as anthropogenic emissions. The influence of climate change from the preindustrial to the present day is also omitted, as all simulations use 2005 meteorology. While this estimate of total net RF is derived using methods that differ from the ACCMIP and IPCC AR5 standard RF definitions, which are present day relative to the year 1850 and 1750, respectively, it provides an opportunity to compare with other studies. This RF is ~66 % of the ACCMIP multimodel mean global net RF of NMVOC emissions for 1850–2000 due to O_3 and CH_4 changes alone ($0.057\,W\,m^{-2}$) (Stevenson et al., 2013), and 15 to 18 % of previous $CO + NMVOC$ RF estimates: $0.25 \pm 0.04\,W\,m^{-2}$ (Shindell et al., 2009) and $0.21 \pm 0.1\,W\,m^{-2}$ (Shindell et al., 2005; Forster et al., 2007). The RF of anthropogenic NMVOCs is ~2.4 % of global net RF of CO_2 ($1.56\,W\,m^{-2}$), and among the positive short-lived forcing agents (CO, CH_4, NMVOCs, and BC), ~2.4 % of their total RF ($1.57\,W\,m^{-2}$) (Forster et al., 2007).

Across the 10 regions, the global annual average net RF, normalized per unit change in NMVOC emissions, is $0.30 \pm 0.15\,mW\,m^{-2}\,(Tg\,C\,yr^{-1})^{-1}$ (mean $\pm$ 1 standard deviation), suggesting variability in the forcings due to different regions' emissions. The normalized RF is most sensitive to NMVOC emissions from regions in the tropics and SH (ME, AU, AF, and IN). Monthly global net RF estimates vary from

Table 4. Annual net RF globally and by latitude band (mW m^{-2}) and GWP$_{20}$ and GWP$_{100}$ estimates for the global and regional reduction simulations relative to the base, due to changes in tropospheric steady-state O$_3$, CH$_4$, and SO$_4^{2-}$ concentrations. Global annual net RF per unit change in NMVOC emissions (mW m^{-2} (Tg C yr^{-1})$^{-1}$) is also shown. The 10 regions estimate represents the sum of the net RFs from all 10 regional reductions; this estimate is not directly estimated by the RTM.

Reduction region	Global annual net RF	Global annual net RF per Tg NMVOC	Annual net RF 90° S–28° S	Annual net RF 28° S–28° N	Annual net RF 28° N–60° N	Annual net RF 60° N–90° N	GWP$_{20}$	GWP$_{100}$
NA	−1.50	0.30	−1.19	−2.13	−0.46	−2.09	9.20	3.27
SA	−1.17	0.35	−0.63	−1.20	−1.98	−1.38	8.56	3.86
EU	−0.70	0.19	−0.69	−1.46	1.05	−1.16	5.36	2.05
FSU	−0.51	0.20	−0.48	−1.05	0.58	−0.71	5.96	2.24
AF	−1.56	0.38	−1.24	−1.99	−1.79	−1.17	11.8	4.19
IN	−1.38	0.37	−0.83	−2.12	−1.54	−0.96	12.7	4.08
EA	−0.05	0.0045	−1.41	−0.24	5.98	−3.30	−1.13	0.079
SE	−1.23	0.29	−1.24	−0.79	−1.85	−1.39	7.58	3.23
AU	−0.13	0.40	0.016	−0.25	−0.21	−0.14	10.5	4.41
ME	−4.22	0.55	−2.29	−6.80	−4.56	−3.06	18.9	6.05
Global	−9.73	0.21	−8.36	−13.8	−1.21	−14.0	5.83	2.36
10 regions	−12.5	0.28	−9.98	−18.0	−4.77	−15.3	–	–

0.03 to 3.5 times the annual mean (excluding EA, which has even greater variability), with the greatest negative RFs from June to August (Fig. S17).

Regional reductions in NMVOC emissions cause widespread negative net RFs (cooling) across both hemispheres from decreases in global CH$_4$ and long-term O$_3$ (Fig. 4). Negative RFs over several source regions (e.g., IN, ME) result from short-term O$_3$ decreases and regional SO$_4^{2-}$ increases (Fig. 3). Regional positive RFs (warming) arise from regional SO$_4^{2-}$ decreases (e.g., NA, EU, FSU, EA, and SE reductions) (Fig. 3), which can oppose the negative RFs of O$_3$ decreases, and tropospheric O$_3$ increases (e.g., SA, AF, SE, and AU reductions) (Fig. 2). These influences are supported by the distributions of changes in longwave radiation (Fig. S18), dominated by O$_3$ and CH$_4$ changes, and shortwave radiation (Fig. S19), dominated by SO$_4^{2-}$. Since the RTM does not calculate the RF of SOA and NO$_3^-$ aerosols presently, our simulated net RFs omit these forcing contributions. If changes in SOA and NO$_3^-$ were accounted for by the RTM, tropospheric SOA decreases (greater than SO$_4^{2-}$ changes in some regions) would likely add small regional warming, while tropospheric NO$_3^-$ increases and decreases (mostly lesser than SO$_4^{2-}$ changes) would add slight regional cooling and warming effects. Globally, NO$_3^-$ and SOA would contribute small negative and positive RFs, respectively, to global net RF. Previous modeling studies have estimated NO$_3^-$ RF as −0.06 W m^{-2} (Bauer et al., 2007) and SOA RF as −0.06 to −0.09 W m^{-2} (Hoyle et al., 2009), for the present day relative to the preindustrial, both of which are small compared to greenhouse gas forcings like tropospheric O$_3$ (0.41 W m^{-2}) (Stevenson et al., 2013).

Using the methods of Collins et al. (2013) and Fry et al. (2012, 2013), we calculate GWPs for each reduction as

the RF integrated to 20 and 100 yr, normalized by the emissions change, and divided by the equivalent for CO$_2$ (Table 4). These GWPs represent short-term contributions from SO$_4^{2-}$ and O$_3$ (assumed constant over one year and zero thereafter), and long-term contributions of CH$_4$ and O$_3$ (responding and decaying with the CH$_4$ perturbation lifetime of 12.48 yr) (Fry et al., 2013). The long-term O$_3$ RF component is calculated by scaling the O$_3$ RF from the CH$_4$ control simulation by the ratio of the long-term O$_3$ burden change from each perturbation to that of the CH$_4$ control. Short-term O$_3$ RF is the difference between steady-state O$_3$ RF (simulated by the RTM) and long-term O$_3$ RF.

GWP$_{20}$ and GWP$_{100}$ are estimated as 5.83 and 2.36, respectively, for the global reduction, and -1.13 to 18.9 and 0.079 to 6.05 among the 10 regions, suggesting strong dependence on emission location, consistent with the normalized net RFs (Fig. 5). GWP$_{20}$ and GWP$_{100}$ are greatest for ME, which also had the largest net RF sensitivity, and smallest for EA, because of the nearly equivalent (opposing) short- and long-term effects. SA, SE, and AU reductions yield the largest (negative) short-term components for GWP$_{20}$ and GWP$_{100}$ due to the combined effect of SO$_4^{2-}$ and tropospheric O$_3$ increases, which act in the opposite direction to the long-term component. Uncertainty in NMVOC GWPs is based on the spread across an ensemble of global CTMs from Fry et al. (2012) (± 1 standard deviation, GWP$_{20}$: ± 6.0 and GWP$_{100}$: ± 2.1), but do not account for the full uncertainty, as additional forcings could change net RF and GWP estimates. The signs of the total global net RF and GWPs are mostly positive, as they represent the overall warming effect of present-day anthropogenic NMVOCs compared to the preindustrial, in contrast to the negative global annual average net RFs (Table 4) due to reductions in NMVOC emissions.
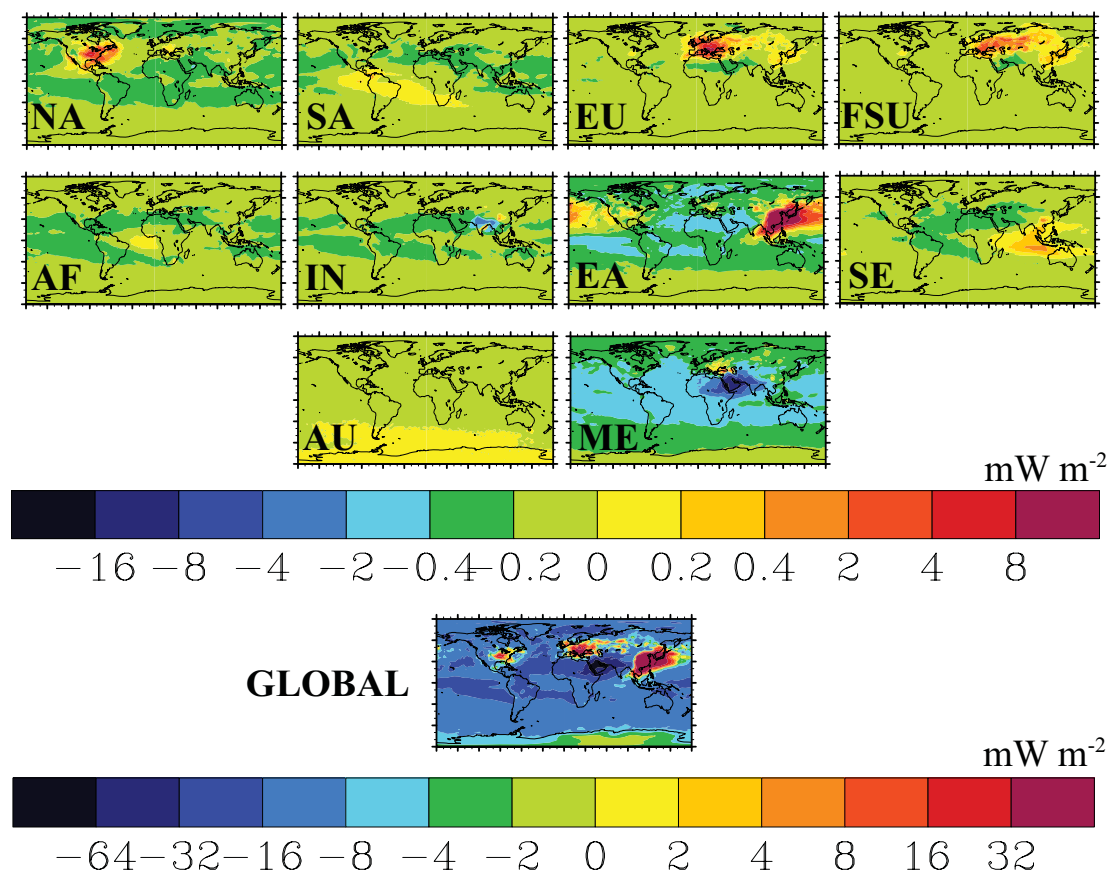
Fig. 4. Annual average net RF distributions (mW m^{-2}) due to changes in tropospheric steady-state O$_3$, CH$_4$, and SO$_4^{2-}$ for the regional and global NMVOC reduction simulations minus the base simulation.

Our GWPs (and RFs) do not include the forcing from CO$_2$ as NMVOCs oxidize, since carbon emissions are often accounted for in CO$_2$ inventories (Fuglestvedt et al., 1996; Daniel and Solomon, 1998; Collins et al., 2002). Including CO$_2$ forcing, however, may provide a more complete accounting of the effects of NMVOCs, increasing each GWP$_{20}$ and GWP$_{100}$ estimate by 3.67 (44 g CO$_2$ mol^{-1} (56.6 g C mol^{-1})$^{-1}$ ·4.7 C per NMVOC molecule), based on the global annual average molecular weight and number of carbons per molecule for anthropogenic NMVOC emissions. This increases the global GWP$_{20}$ and GWP$_{100}$ by 63 % and 155 %, respectively, and makes all regional GWP$_{20}$ and GWP$_{100}$ estimates positive.

The GWP$_{20}$ and GWP$_{100}$ estimates for NA, EU, and IN (South Asia) reductions are approximately 32 to 41 %, 61 to 69 %, and 50 to 52 % lower than the multimodel mean estimates of Fry et al. (2012) (Table S10). EA GWP$_{20}$ and GWP$_{100}$ estimates, being near zero, also greatly contrast with Fry et al. (2012). Here total NMVOC/NO$_x$ emissions ratios are 57 % greater globally and in NA than the multimodel mean ratios, partly due to greater biogenic NMVOC emissions (calculated online in MOZART-4) for the year 2005. The multimodel ensemble evaluated by Fry et al. (2012) uti-

lizes an emissions inventory representative of the year 2001. In EU, EA, and IN, the total NMVOC/NO$_x$ emissions are closer to the multimodel mean ratios: 4 % and 9 % (EU and EA, respectively) less and 8 % (IN) greater than those of the multimodel mean (Table S11). Global O$_3$ burden responses (in Tg O$_3$ (Tg C yr^{-1})$^{-1}$) are 27 % to 51 % less than those in Fry et al. (2012), likely due to the greater NMVOC/NO$_x$ emission ratios in this study, which would suggest less sensitivity to NMVOC emissions, but differences in the representations of NMVOCs and oxidation chemistry among models may also contribute to these differences. Global SO$_4^{2-}$ responses (in Gg SO$_4^{2-}$ (Tg C yr^{-1})$^{-1}$) also highly vary, more commonly causing increases in SO$_4^{2-}$ compared to the decreases in Fry et al. (2012) (Table S12). Collins et al. (2002) calculated GWP$_{100}$ estimates for individual NMVOC species (due to CH$_4$ and O$_3$ only) ranging from 1.9 to 5.5 (−50 % to 100 % uncertainty), which are more similar to the GWP$_{100}$ magnitudes estimated here. While our NMVOC GWP estimates consider all anthropogenic NMVOCs together and are derived from only one CTM and RTM, they represent emissions from a greater number of regions, including the tropics and extra-tropics.
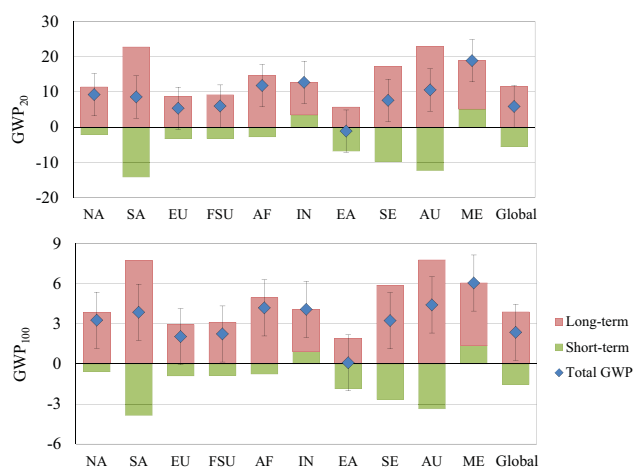
Fig. 5. Global warming potentials for NMVOCs at time horizons of 20 and 100 yr (GWP_{20}, GWP_{100}) for the regional and global reductions, with contributions from short-term (O_3 and SO_4^{2-}) and long-term (O_3 and CH_4) components, where total GWP is short-term + long-term. Uncertainty bars represent the average uncertainty found by Fry et al. (2012) based on the spread of atmospheric chemical models (± 1 standard deviation).

5   Summary

Reducing NMVOC emissions provides regional to global benefits to air quality and climate. Halving anthropogenic NMVOCs from each region creates widespread small negative net RFs across both hemispheres from global CH_4 and long-term O_3 decreases. RF is also negative near several source regions (e.g., IN, ME) due to regional SO_4^{2-} increases and short-term O_3 decreases. Regional small positive RFs correspond to regional SO_4^{2-} decreases (e.g., NA, EU, FSU, EA, and SE) and tropospheric O_3 increases (e.g., SA, AF, SE, and AU).

The global annual average net RF for the global 50 % NMVOC reduction is estimated as $-9.73\,\mathrm{mW\,m^{-2}}$ or $0.21\,\mathrm{mW\,m^{-2}}$ $(\mathrm{Tg\,C\,yr^{-1}})^{-1}$. Our RF, GWP_{20}, and GWP_{100} estimates for the NA, EA, EU, and IN reductions are lower than the multimodel mean estimates of Fry et al. (2012), due to differences in O_3-NO_x-VOC sensitivities and SO_4^{2-} responses, and in particular, because of regional O_3 increases and SO_4^{2-} decreases for some regions that oppose the long-term cooling. Considerable variability in the global net RF, GWP_{20}, and GWP_{100} estimates among regions suggests a strong dependence on emission location: $0.21\,\mathrm{mW\,m^{-2}}$ $(\mathrm{Tg\,C\,yr^{-1}})^{-1}$, 5.83, and 2.36 for the global reduction, and $0.30 \pm 0.15\,\mathrm{mW\,m^{-2}}$ $(\mathrm{Tg\,C\,yr^{-1}})^{-1}$, -1.13 to 18.9, and 0.079 to 6.05 for the 10 regions. GWP_{20} and GWP_{100} are greatest for regions in the tropics and SH (i.e., ME, IN, and AF) and less for regions in the northern midlatitudes (i.e., EU and FSU). The lowest GWP_{20} and GWP_{100} estimates are for EA, given the nearly equivalent (opposing) short- and long-term effects. Including additional forc-

ings beyond CH_4, O_3, and SO_4^{2-} would likely change RF and GWP estimates.

Variability in global annual average tropospheric CH_4, O_3, and SO_4^{2-} responses contributes to the RF and GWP differences seen among regions: 0.81 ppbv CH_4 $(\mathrm{Tg\,C\,yr^{-1}})^{-1}$, 0.073 Tg O_3 $(\mathrm{Tg\,C\,yr^{-1}})^{-1}$, and 0.33 Gg SO_4^{2-} $(\mathrm{Tg\,C\,yr^{-1}})^{-1}$ for the global reduction, and 0.40 to 1.61 ppbv CH_4 $(\mathrm{Tg\,C\,yr^{-1}})^{-1}$, -0.008 to 0.101 Tg O_3 $(\mathrm{Tg\,C\,yr^{-1}})^{-1}$, and -0.21 to 1.01 Gg SO_4^{2-} $(\mathrm{Tg\,C\,yr^{-1}})^{-1}$ among the 10 regions. Several regions with high GWPs are low-NO_x regions (AF and AU), which have stronger CH_4 sensitivities to NMVOC reductions, and weak increases or decreases in SO_4^{2-}.

Anthropogenic NMVOC emissions overall contribute $\sim$5.1 % (1.9 ppbv) to global annual average steady-state surface O_3, by doubling the change from the 50 % global NMVOC reduction (-0.67 ppbv) and scaling for biomass burning emissions. Some regional reductions contribute importantly to surface O_3 in other regions, such as EA, ME, and EU, which impact US surface O_3 by 43 %, 34 %, and 34 %, respectively, of that from NA emissions. NMVOC emission reductions mostly have a greater impact on downwind O_3 production than the formation and export of O_3 from each source region. Long-term surface O_3 changes (via CH_4) impact air quality globally, and for most regions add 5–18 % to short-term changes.

In this study, the air quality and RF impacts are derived from one CTM and RTM, which limits our ability to capture a more complete range of CH_4, O_3, aerosols, and RF responses, as a model ensemble would. Previous studies have shown a large model spread in CH_4, O_3, and SO_4^{2-} responses to regional NMVOC emissions (Collins et al., 2002; Fiore et al., 2009; Fry et al., 2012). Future work could examine the emissions inventories of NMVOCs and other species, as they are fairly uncertain among models (Berntsen et al., 2005).

Other limitations include only accounting for CH_4, O_3, and SO_4^{2-} (direct effect only) in our net RF and GWP estimates, which may affect the magnitude of our estimates and variability among regions. Forcing mechanisms not accounted for include NO_3^-, SOA, stratospheric O_3, water vapor, the carbon cycle (via O_3 and nitrogen deposition), the indirect effects of aerosols, and the internal mixing of aerosols. Future research could include these additional forcings and their uncertainty. The contribution of anthropogenic NMVOCs to SOA, in particular, is fairly uncertain, and often underpredicted by models (Volkamer et al., 2006). The influence of climate feedbacks on chemistry and future changes in emissions also may alter the air quality and RF sensitivities estimated here for present-day emissions. In addition, while we focus on the sensitivity of air quality and RF to NMVOC emissions, which is useful in determining the GWP of NMVOCs, emission control measures would likely affect co-emitted species. Our results can be combined with those for co-emitted pollutants to evaluate the net

effect of measures affecting multiple pollutants. Full climate responses also could be evaluated, as in Shindell and Faluvegi (2009).

These findings of high variability in GWPs among regions for NMVOCs contrast with our earlier findings for CO, with little variability in GWPs among source regions (Fry et al., 2013). While it would be possible to include CO in multi-gas emissions trading schemes using a single GWP, with little error, using a single GWP for NMVOCs would cause significant error. Instead, international climate agreements could consider including NMVOCs in multi-gas emissions trading schemes using GWPs that are specific to each region. Although NMVOCs are a small climate forcing agent, this study motivates reductions in NMVOC emissions as part of future coordinated policies addressing air quality and climate change (Rypdal et al., 2005, 2009; Jackson et al., 2009; Shindell et al., 2012; Fry et al., 2013).

Supplementary material related to this article is available online at http://www.atmos-chem-phys.net/14/523/2014/acp-14-523-2014-supplement.pdf.

References

Barth, M. C., Rasch, P. J., Kiehl, J. T., Benkovitz, C. M., and Schwartz, S. E.: Sulfur chemistry in the National Center for Atmospheric Research Community Climate Model: Description, evaluation, features, and sensitivity to aqueous chemistry, J. Geophys. Res., 105, 1387–1415, 2000.

Bauer, S. E., Koch, D., Unger, N., Metzger, S. M., Shindell, D. T., and Streets, D. G.: Nitrate aerosols today and in 2030: a global simulation including aerosols and tropospheric ozone, Atmos. Chem. Phys., 7, 5043–5059, doi:10.5194/acp-7-5043-2007, 2007.

Berntsen, T. K., Fuglestvedt, J. S., Joshi, M. M., Shine, K. P., Stuber, N., Ponater, M., Sausen, R., Hauglustaine, D. A., and Li, L.: Response of climate to regional emissions of ozone precursors: sensitivities and warming potentials, Tellus, 57B, 283–304, doi:10.1111/j.1600-0889.2005.00152.x, 2005.

Berntsen, T. K., Fuglestvedt, J., Myhre, G., Stordal, F., and Bergle, T. F.: Abatement of greenhouse gases: Does location matter?,

Climatic Change, 74, 377–411, doi:10.1007/s10584-006-0433-4, 2006.

Carlton, A. G., Wiedinmyer, C., and Kroll, J. H.: A review of Secondary Organic Aerosol (SOA) formation from isoprene, Atmos. Chem. Phys., 9, 4987–5005, doi:10.5194/acp-9-4987-2009, 2009.

Chung, S. and Seinfeld, J.: Global distribution and climate forcing of carbonaceous aerosols, J. Geophys. Res., 107, 4407, doi:10.1029/2001JD001397, 2002.

Cionni, I., Eyring, V., Lamarque, J.-F., Randel, W. J., Stevenson, D. S., Wu, F., Bodeker, G. E., Shepherd, T. G., Shindell, D. T., and Waugh, D. W.: Ozone database in support of CMIP5 simulations: results and corresponding radiative forcing, Atmos. Chem. Phys., 11, 11267–11292, doi:10.5194/acp-11-11267-2011, 2011.

Collins, W. J., Derwent, R. G., Johnson, C. E., and Stevenson, D. S.: The oxidation of organic compounds in the troposphere and their global warming potentials, Climatic Change, 52, 453-479, doi:10.1023/A:1014221225434, 2002.

Collins, W. J., Fry, M. M., Yu, H., Fuglestvedt, J. S., Shindell, D. T., and West, J. J.: Global and regional temperature-change potentials for near-term climate forcers, Atmos. Chem. Phys., 13, 2471–2485, doi:10.5194/acp-13-2471-2013, 2013.

Daniel, J. S. and Solomon, S.: On the climate forcing of carbon monoxide, J. Geophys. Res., 103, 13249–13260, doi:10.1029/98JD00822, 1998.

Ehhalt, D., Prather, M., Dentener, F., Derwent, R., Dlugokencky, E., Holland, E., Isaksen, I., Katima, J., Kirchhoff, V., Matson, P., Midgley, P., and Wang, M.: Atmospheric chemistry and greenhouse gases, in: Climate Change 2001: The Scientific Basis, Contribution of Working Group I to the Third Assessment Report of the Intergovernmental Panel on Climate Change, edited by: Houghton, J. T., Ding, Y., Griggs, D. J., Noguer, M., van der Linden, P. J., Dai, X., Maskell, K., and Johnson, C. A., Cambridge University Press, Cambridge, UK, 257–259, 2001.

Emmons, L. K., Walters, S., Hess, P. G., Lamarque, J.-F., Pfister, G. G., Fillmore, D., Granier, C., Guenther, A., Kinnison, D., Laepple, T., Orlando, J., Tie, X., Tyndall, G., Wiedinmyer, C., Baughcum, S. L., and Kloster, S.: Description and evaluation of the Model for Ozone and Related chemical Tracers, version 4 (MOZART-4), Geosci. Model Dev., 3, 43–67, doi:10.5194/gmd-3-43-2010, 2010.

Fiore, A. M., Jacob, D. J., Field, B. D., Streets, D. G., Fernandes, S. D., and Jang, C.: Linking ozone pollution and climate change: The case for controlling methane, Geophys. Res. Lett., 29, 1919, doi:10.1029/2002GL015601, 2002.

Fiore, A. M., Dentener, F. J., Wild, O., Cuvelier, C., Schultz, M. G., Hess, P., Textor, C., Schulz, M., Doherty, R. M., Horowitz, L. W., MacKenzie, I. A., Sanderson, M. G., Shindell, D. T., Stevenson, D. S., Szopa, S., Van Dingenen, R., Zeng, G., Atherton, C., Bergmann, D., Bey, I., Carmichael, G., Collins, W. J., Duncan, B. N., Faluvegi, G., Folberth, G., Gauss, M., Gong, S., Hauglustaine, D., Holloway, T., Isaksen, I. S. A., Jacob, D. J., Jonson, J. E., Kaminski, J. W., Keating, T. J., Lupu, A., Marmer, E., Montanaro, V., Park, R. J., Pitari, G., Pringle, K. J., Pyle, J. A., Schroeder, S., Vivanco, M. G., Wind, P., Wojcik, G., Wu, S., and Zuber, A.: Multimodel estimates of intercontinental source-receptor relationships for ozone pollution, J. Geophys. Res., 114, D04301, doi:10.1029/2008JD010816, 2009.

Forster, P., Ramaswamy, V., Artaxo, P., Berntsen, T., Betts, R., Fahey, D. W., Haywood, J., Lean, J., Lowe, D. C., Myhre, G., Nganga, J., Prinn, R., Raga, G., Schulz, M., and Van Dorland, R.: Changes in atmospheric constituents and in radiative forcing, in: Climate Change 2007: The Physical Science Basis. Contribution of Working Group I to the Fourth Assessment Report of the Intergovernmental Panel on Climate Change, edited by: Solomon, S., Qin, D., Manning, M., Chen, Z., Marquis, M., Averyt, K. B., Tignor, M., and Miller, H. L., Cambridge Univ. Press, Cambridge, UK, 129–234, 2007.

Fry, M. M., Naik, V., West, J. J., Schwarzkopf, M. D., Fiore, A. M., Collins, W. J., Dentener, F. J., Shindell, D. T., Atherton, C., Bergmann, D., Duncan, B. N., Hess, P., MacKenzie, I. A., Marmer, E., Schultz, M. G., Szopa, S., Wild, O., and Zeng, G.: The influence of ozone precursor emissions from four world regions on tropospheric composition and radiative climate forcing, J. Geophys. Res., 117, D07306, doi:10.1029/2011JD017134, 2012.

Fry, M. M., Schwarzkopf, M. D., Adelman, Z., Naik, V., Collins, W. J., and West, J. J.: Net radiative forcing and air quality responses to regional CO emission reductions, Atmos. Chem. Phys., 13, 5381–5399, doi:10.5194/acp-13-5381-2013, 2013.

Fuglestvedt, J. S., Isaksen, I. S. A., and Wang, W.-C.: Estimates of indirect global warming potentials for CH_4, CO, and NO_x. Clim. Change, 34, 405–437, 1996.

GFDL Global Atmospheric Model Development Team (GAMDT): The new GFDL global atmosphere and land model AM2-LM2: Evaluation with prescribed SST simulations, J. Clim., 17, 4641–4673, 2004.

Guenther, A., Karl, T., Harley, P., Wiedinmyer, C., Palmer, P. I., and Geron, C.: Estimates of global terrestrial isoprene emissions using MEGAN (Model of Emissions of Gases and Aerosols from Nature), Atmos. Chem. Phys., 6, 3181–3210, doi:10.5194/acp-6-3181-2006, 2006.

Hoyle, C. R., Myhre, G., Berntsen, T. K., and Isaksen, I. S. A.: Anthropogenic influence on SOA and the resulting radiative forcing, Atmos. Chem. Phys., 9, 2715–2728, doi:10.5194/acp-9-2715-2009, 2009.

Ito, A., Sillman, S., and Penner, J. E.: Effects of additional nonmethane volatile organic compounds, organic nitrates, and direct emissions of oxygenated organic species on global tropospheric chemistry, J. Geophys. Res., 112, D06309, doi:10.1029/2005JD006556, 2007.

Jackson, S. C.: Parallel Pursuit of Near-term and Long-term Climate Mitigation, Science, 326, 5952, 526-527, doi:10.1126/science.1177042, 2009.

Jacob, D. J.: Introduction to Atmospheric Chemistry, Princeton University Press, Princeton, NJ, USA, 52–53, 1999.

Lamarque, J.-F., Kiehl, J. T., Hess, P. G., Collins, W. D., Emmons, L. K., Ginoux, P., Luo, C., and Tie, X. X.: Response of a coupled chemistry-climate model to changes in aerosol emissions: Global impact on the hydrological cycle and the tropospheric burdens of OH, ozone, and NO_x, Geophys. Res. Lett., 32, L16809, doi:10.1029/2005GL023419, 2005.

Leibensperger, E. M., Mickley, L. J., Jacob, D. J., and Barrett, S. R. H.: Intercontinental influence of NO_x and CO emissions on particulate matter air quality, Atmos Environ., 45, 3318–3324, doi:10.1016/j.atmosenv.2011.02.023, 2011.

Liu, X.-H., Zhang, Y., Xing, J., Zhang, Q., Wang, K., Streets, D. G., Jang, C., Wang, W.-X., and Hao, J.-M.: Understanding of regional air pollution over China using CMAQ, part II. Process analysis and sensitivity of ozone and particulate matter to precursor emissions, Atmos. Environ., 44, 3719–3727, 2010.

Meinshausen, M., Smith, S. J., Calvin, K. V., Daniel, J. S., Kainuma, M. L. T., Lamarque, J.-F., Matsumoto, K., Montzka, S. A., Raper, S. C. B., Riahi, K., Thomson, A. M., Velders, G. J. M., and van Vuuren, D.: The RCP Greenhouse Gas Concentrations and their Extension from 1765 to 2300, Climatic Change (Special Issue), 109, 213–241, doi:10.1007/s10584-011-0156-z, 2011.

Metzger, S., Dentener, F., Pandis, S., and Lelieveld, J.: Gas/aerosol partitioning: 1. A computationally efficient model, J. Geophys. Res., 107, 4312, doi:10.1029/2001JD001102, 2002.

Naik, V., Mauzerall, D., Horowitz, L., Schwarzkopf, M. D., Ramaswamy, V., and Oppenheimer, M.: Net radiative forcing due to changes in regional emissions of tropospheric ozone precursors, J. Geophys. Res., 110, D24306, doi:10.1029/2005JD005908, 2005.

Naik, V., Mauzerall, D. L., Horowitz, L. W., Schwarzkopf, M. D., Ramaswamy, V., and Oppenheimer, M.: On the sensitivity of radiative forcing from biomass burning aerosols and ozone to emission location, Geophys. Res. Lett., 34, L03818, doi:10.1029/2006GL028149, 2007.

Prather, M., Ehhalt, D., Dentener, F., Derwent, R. G., Dlugokencky, E., Holland, E., Isaksen, I. S. A., Katima, J., Kirchhoff, V., Matson, P., Midgley, P. M., and Wang, M.: Climate Change 2001: The Scientific Basis, Atmospheric Chemistry and Greenhouse Gases, Chap. 4, Cambridge Univ. Press, New York, USA, 239–287, 2001.

Prather, M. J.: Time scales in atmospheric chemistry: Theory, GWPs for CH_4 and CO, and runaway growth, Geophys. Res. Lett., 23, 2597–2600, doi:10.1029/96GL02371, 1996.

Riahi, K., Gruebler, A., and Nakicenovic, N.: Scenarios of long-term socio-economic and environmental development under climate stabilization, Technological Forecasting and Social Change, 74, 7, 887–935, 2007.

Riahi, K., Rao, S., Krey, V., Cho, C., Chirkov, V., Fischer, G., Kindermann, G., Nakicenovic, N., and Rafaj, P.: RCP 8.5 – A scenario of comparatively high greenhouse gas emissions, Climatic Change, 109, 33–57, doi:10.1007/s10584-011-0149-y, 2011.

Rienecker, M. M., Suarez, M. J., Todling, R., Bacmeister, J., Takacs, L., Liu, H.-C., Gu, W., Sienkiewicz, M., Koster, R. D., Gelaro, R., Stajner, I., and Nielsen, J. E.: The GEOS-5 Data Assimilation System – Documentation of versions 5.0.1, 5.1.0, and 5.2.0, NASA Tech. Memo., NASA/TM–2008–104606, vol. 27, 118 pp., 2008.

Rypdal, K., Berntsen, T., Fuglestvedt, J. S., Aunan, K., Torvanger, A., Stordal, F., Pacyna, J. M., and Nygaard, L. P.: Tropospheric ozone and aerosols in climate agreements: scientific and political challenges, Environ. Sci. Policy, 8, 29–43, doi:10.1016/j.envsci.2004.09.003, 2005.

Rypdal, K., Rive, N., Berntsen, T., Fagerli, H., Klimont, Z., Mideksa, T. K., and Fuglestvedt, J. S.: Climate and air quality-driven scenarios of ozone and aerosol precursor abatement, Environ. Sci. Policy, 12, 855–869, doi:10.1016/j.envsci.2009.08.002, 2009.

Saikawa, E., Naik, V., Horowitz, L. W., Liu, J. F., and Mauzerall, D. L.: Present and potential future contributions of sulfate, black and

organic carbon aerosols from China to global air quality, premature mortality and radiative forcing, Atmos. Environ., 43, 2814–2822, doi:10.1016/j.atmosenv.2009.02.017, 2009.

Schwarzkopf, M. D. and Ramaswamy, V.: Radiative effects of CH_4, N_2O, halocarbons and the foreign-broadened H_2O continuum: A GCM experiment, J. Geophys. Res., 104, 9467–9488, doi:10.1029/1999JD900003, 1999.

Shindell, D. and Faluvegi, G.: Climate response to regional radiative forcing during the twentieth century, Nature Geosci., 2, 294–300, doi:10.1038/NGEO473, 2009.

Shindell, D., Kuylenstierna, J. C. I., Vignati, E., van Dingenen, R., Amann, M., Klimont, Z., Anenberg, S. C., Muller, N., Janssens-Maenhout, G., Raes, F., Schwartz, J., Faluvegi, G., Pozzoli, L., Kupiainen, K., Höglund-Isaksson, L., Emberson, L., Streets, D., Ramanathan, V., Hicks, K., Oanh, N. T. K., Milly, G., Williams, M., Demkine, V., and Fowler, D.: Simultaneously mitigating near-term climate change and improving human health and food security. Science, 335, 183–189, doi:10.1126/science.1210026, 2012.

Shindell, D. T., Faluvegi, G., Bell, N., and Schmidt, G. A.: An emissions-based view of climate forcing by methane and tropospheric ozone, Geophys. Res. Lett., 32, L04803, doi:10.1029/2004GL021900, 2005.

Shindell, D. T., Faluvegi, G., Koch, D. M., Schmidt, G. A., Unger, N., and Bauer, S. E.: Improved attribution of climate forcing to emissions, Science, 326, 716–718, doi:10.1126/science.1174760, 2009.

Shindell, D. T., Lamarque, J.-F., Schulz, M., Flanner, M., Jiao, C., Chin, M., Young, P. J., Lee, Y. H., Rotstayn, L., Mahowald, N., Milly, G., Faluvegi, G., Balkanski, Y., Collins, W. J., Conley, A. J., Dalsoren, S., Easter, R., Ghan, S., Horowitz, L., Liu, X., Myhre, G., Nagashima, T., Naik, V., Rumbold, S. T., Skeie, R., Sudo, K., Szopa, S., Takemura, T., Voulgarakis, A., Yoon, J.-H., and Lo, F.: Radiative forcing in the ACCMIP historical and future climate simulations, Atmos. Chem. Phys., 13, 2939–2974, doi:10.5194/acp-13-2939-2013, 2013.

Sillman, S., He, D., Cardelino, C., and Imhoff, R. E.: The use of photochemical indicators to evaluate ozone-NOx-hydrocarbon sensitivity: Case studies from Atlanta, New York, and Los Angeles, J. Air Waste Manage. Assoc., 47, 1030–1040, 1997.

Søvde, O. A., Hoyle, C. R., Myhre, G., and Isaksen, I. S. A.: The HNO_3 forming branch of the HO_2+NO reaction: pre-industrial-to-present trends in atmospheric species and radiative forcings, Atmos. Chem. Phys., 11, 8929–8943, doi:10.5194/acpd-11-8929-2011, 2011.

Stevenson, D. S., Dentener, F. J., Schultz, M. G., Ellingsen, K., van Noije, T. P. C., Wild, O., Zeng, G., Amann, M., Atherton, C. S., Bell, N., Bergmann, D. J., Bey, I., Butler, T., Cofala, J., Collins, W. J., Derwent, R. G., Doherty, R. M., Drevet, J., Eskes, H. J., Fiore, A. M., Gauss, M., Hauglustaine, D. A., Horowitz, L. W., Isaksen, I. S. A., Krol, M. C., Lamarque, J.-F., Lawrence, M. G., Montanaro, V., Müller, J.-F., Pitari, G., Prather, M. J., Pyle, J. A., Rast, S., Rodriguez, J. M., Sanderson, M. G., Savage, N. H., Shindell, D. T., Strahan, S. E., Sudo, K., and Szopa, S.: Multimodel ensemble simulations of present-day and near-future tropospheric ozone, J. Geophys. Res., 111, D08301, doi:10.1029/2005JD006338, 2006.

Stevenson, D. S., Young, P. J., Naik, V., Lamarque, J.-F., Shindell, D. T., Voulgarakis, A., Skeie, R. B., Dalsoren, S. B., Myhre, G., Berntsen, T. K., Folberth, G. A., Rumbold, S. T., Collins, W. J., MacKenzie, I. A., Doherty, R. M., Zeng, G., van Noije, T. P. C., Strunk, A., Bergmann, D., Cameron-Smith, P., Plummer, D. A., Strode, S. A., Horowitz, L., Lee, Y. H., Szopa, S., Sudo, K., Nagashima, T., Josse, B., Cionni, I., Righi, M., Eyring, V., Conley, A., Bowman, K. W., Wild, O., and Archibald, A.: Tropospheric ozone changes, radiative forcing and attribution to emissions in the Atmospheric Chemistry and Climate Model Intercomparison Project (ACCMIP), Atmos. Chem. Phys., 13, 3063–3085, doi:10.5194/acp-13-3063-2013, 2013.

Unger, N., Shindell, D. T., Koch, D. M., and Streets, D. G.: Cross influences of ozone and sulfate precursor emissions changes on air quality and climate, Proc. Natl. Acad. Sci., 103, 12, 4377–4380, doi:10.1073/pnas.0508769103, 2006.

Volkamer, R., Jimenez, J. L., San Martini, F., Dzepina, K., Zhang, Q., Salcedo, D., Molina, L. T., Worsnop, D. R., and Molina, M. J.: Secondary organic aerosol formation from anthropogenic air pollution: Rapid and higher than expected, Geophys. Res. Lett., 33, L17811, doi:10.1029/2006GL026899, 2006.

West, J. J., Fiore, A. M., Naik, V., Horowitz, L. W., Schwarzkopf, M. D., and Mauzerall, D. L.: Ozone air quality and radiative forcing consequences of changes in ozone precursor emissions, Geophys. Res. Lett., 34, L06806, doi:10.1029/2006GL029173, 2007.

West, J. J., Naik, V., Horowitz, L. W., and Fiore, A. M.: Effect of regional precursor emission controls on long-range ozone transport – Part 1: Short-term changes in ozone air quality, Atmos. Chem. Phys., 9, 6077–6093, doi:10.5194/acp-9-6077-2009, 2009a.

West, J. J., Naik, V., Horowitz, L. W., and Fiore, A. M.: Effect of regional precursor emission controls on long-range ozone transport – Part 2: Steady-state changes in ozone air quality and impacts on human mortality, Atmos. Chem. Phys., 9, 6095-6107, doi:10.5194/acp-9-6095-2009, 2009b.

Wild, O., Prather, M. J., and Akimoto, H.: Indirect long-term global radiative cooling from NO_x emissions, Geophys. Res. Lett., 28, 1719–1722, doi:10.1029/2000GL012573, 2001.

World Meteorological Organization (WMO): WMO Greenhouse Gas Bulletin: The State of Greenhouse Gases in the Atmosphere using Global Observations through 2005, Bulletin No. 1: March 2006, 2006.